An Enhanced Molecular Dynamics Study of HPPK−ATP Conformation Space Exploration and ATP Binding to HPPK†

Li Su and Robert I. Cukier*

Department of Chemistry, Michigan State University, East Lansing, Michigan 48824-1322

Received: September 30, 2008; Revised Manuscript Received: December 10, 2008

HPPK (6-hydroxymethyl-7,8-dihydropterin pyrophosphokinase) catalyzes the transfer of pyrophosphate from ATP to HP (6-hydroxymethyl-7,8-dihydropterin). This first reaction in the folate biosynthetic pathway is an important target for potential antimicrobial agents. In this work, the mechanism by which HPPK traps and binds ATP is studied by molecular dynamics (MD)-based methods. Based on the ternary crystal structure of HPPK with an ATP mimic and HP, a complex of $ATPMg_2$ and HPPK is simulated and found to undergo small conformational changes with conventional MD, as does also conventional MD when started from the apo crystal structure. The introduction of restraints in the MD that serve to move HPPK−ATP from its ternary complex (closed) to apo-like (open) forms shows that throughout the restraint path ATP remains bound to HPPK. That ATP remains bound suggests that there is an ensemble of conformations with ATP bound to HPPK that span the apo to more ligand-bound-like conformations, consistent with the pre-existing equilibrium hypothesis of ligand binding, whereby a ligand can select from and bind to a broad range of protein conformations. In the apo-like conformations, $ATPMg_2$ remains bound to HPPK through a number of mainly salt-bridge-like interactions between several negatively charged residues and the two magnesium cations. The introduction of a reweight method that enhances the sampling of MD by targeting explicit terms in the force field helps define the interactions that bind ATP to HPPK. Using the reweight method, conformational and center of mass motions of ATP, driven by the breaking and making of hydrogen bonds and salt bridges, are identified that lead to ATP separating from HPPK. An elastic normal mode (ENM) approach to opening the ternary complex and closing the apo crystal structures was carried out. The ENM analysis of the apo structure analysis shows one mode that does have a closing motion of HPPK loops, but the direction does not correlate strongly with the loop motions that are required for forming the ternary complex.

1. Introduction

Mechanistic proposals of how proteins (enzymes) bind their ligands to carry out chemical transformations have a long history. A progression of models has been introduced that in essence increases the role of protein plasticity in the binding of ligands.[1−4] The "lock and key" concept, introduced by Fischer, asserts that a protein has a cavity that a ligand (or another protein) can be fit into with minor rearrangements of protein and ligand. This model does not account for proteins that can bind differently shaped substrates. Koshland's "induced fit" model tries to account for this by suggesting that a ligand induces a conformational change at the binding site, shifting it toward an active state. The pre-existing equilibrium hypothesis,[5] based on more recent funnel energy landscape protein-folding theories,[6,7] asserts that the native state of the protein exhibits an ensemble of conformations that can span apo to more ligand-bound-like conformations. The ligand can select a prebinding conformation and thereby bias the equilibrium toward the catalytically competent binding conformation. Indeed, the Monod−Wyman−Changeux (MWC)[8] model of allosteric regulation relies on the possibility of equilibrium between pre-existing conformations that stresses the view that a protein (without ligands) equilibrates between two distinct conformers. Conformational plasticity may be more advantageous for ligand binding by requiring smaller protein rearrangements (with a reduced energetic requirement) than would be necessary in the more open forms.

This more "dynamic" view of the ligand binding process introduces difficulties for mechanistic studies that are based on crystal structures of various substrate-bound (usually using substrate mimics to prevent enzyme turnover) and apo forms because crystallization gives essentially one conformation and therefore cannot provide evidence for intermediate conformations. NMR structure determination is more suited to such investigations in that it can provide an ensemble of structures. Sometimes a conformational ensemble is found that, for example, provides a rather diverse population of loop conformations. Once the emphasis shifts to conformational ensembles, a natural approach is to use Molecular Dynamics (MD) simulation to generate trajectories of conformations that can be used to address these issues. In this regard, MD stands in contrast to docking approaches where ligands and proteins are mainly considered as rigid objects. Furthermore, even if different protein configurations are used (versus one protein configuration) in the docking procedure, they are typically obtained in the absence of a ligand and therefore do not account for the mutual rearrangement of protein and ligand. However, MD has the distinct disadvantage that integrating Newton's equations of motion with a femtosecond time step will have difficulty reaching times that can capture substantial conformational transitions and fluctuations that may be occurring on the micro to even seconds time scales, due to the complex configuration space that has substantial barriers in the high-dimensional

† Part of the "Max Wolfsberg Festschrift".

* Corresponding author. Phone: (517) 355-9715 ext. 263. Fax: (517) 353-1793. E-mail: cukier@cem.msu.edu.

10.1021/jp808664k CCC: $40.75
Published on Web 02/04/2009

potential energy surface. Thus, various methods of accelerating the ability of MD to explore conformational space such as multicanonical ensemble,[9,10] simulated tempering,[11,12] parallel tempering (replica exchange),[13−21] and reweight methods[22−28] have been proposed.

In this work, we apply some enhanced MD methods to explore the mechanism of substrate binding in the enzyme 6-hydroxymethyl-7,8-dihydropterin pyrophosphokinase (HPPK), which catalyzes the transfer of pyrophosphate from ATP to 6-hydroxymethyl-7,8-dihydropterin (HP). It is the first reaction in the folate biosynthetic pathway.[29] Many kinases that catalyze phosphoryl transfer[30] have been extensively studied, but less is known about the mechanism of pyrophosphokinases. While mammals obtain folates from their diet, most microorganisms must synthesize folates de novo, making the folate biosynthetic pathway an important target for potential antimicrobial agents.[31]

A number of crystal and NMR derived structures of HPPK with ATP mimics and/or HP and HP-based ligands have been obtained. The structure of apo HPPK[32] from *E. coli*, determined by crystallography, reveals a three-layered $\alpha\beta\alpha$ fold formed by six β-strands and four α-helices. There are two highly flexible loops and a third loop that is less flexible. A crystal structure of the ternary complex with AMPCPP and two associated Mg^{2+} ions (AMPCPP is nonreactive analog of ATP) and with HP shows significant conformational changes relative to the apo structure concentrated in the flexible loops[33] that serve to sequester the ligands in a catalytically competent form. Crystal structure data on the binary complex of HPPK with AMPCPP show that this binary complex is trapped in a "superopen" conformation where one of the loops (loop 3) is in an extended conformation.[34] NMR studies of HPPK with a related ATP analog, AMPPCP, which may be a better substrate mimic, present on average a different but also more open (than apo) conformation.[35] Actually, examination of the ensemble of structures reveals that some are in conformations that approach the ternary closed conformation. The NMR results suggest that the binary complex of HPPK with ATP most likely is labile, sampling both open and closed-like conformations. MD simulations of apo HPPK and a binary complex of HPPK with ATP, based on the NMR superopen form, have been carried out.[36] The sampling of the loop conformations was improved with the use of the locally enhanced sampling method (LES).[37] These simulations showed that the apo loop conformations could be quite similar to those found in the experimentally determined superopen binary complex. The LES simulation even produced conformations of loop three that are more open than found in the crystal binary complex structure. Thus, it appears that the loops of HPPK can sample a very broad range of conformations and that HPPK may fall into the category of a pre-existing equilibrium enzyme.

Equilibrium binding measurements show that HPPK binds ATP (actually AMPPCP) with high affinity, and kinetic measurements indicate that ATP binds first, and slowly, followed by very rapid HP binding.[38] Without the presence of ATP, HPPK does not bind HP in measurable quantities. These data suggest that there is a "proto-pocket" for HP binding that is formed by first binding ATP. The slow ATP binding is consistent with the idea that there is conformational flexibility of HPPK and that ATP selects from a conformational ensemble. Once ATP is bound, the HPPK−ATP complex may stabilize to a set of conformations appropriate for the rapid uptake of HP.

Our initial simulations of HPPK focused on the apo crystal structure. We found that conventional MD led to little conformational change. The loops do fluctuate more than the core parts of HPPK, but there was no evidence of loop conformations resembling the ternary structure. Enhanced MD sampling methods did show more conformational changes in the loops, but no definitive evidence for more closed-like conformations evocative of the ternary complex structure. Simulations starting from the ternary structure with both ligands removed essentially fluctuated around the ternary form with no tendency for opening toward the apo structure; if anything, there was a distinct contraction of HPPK related to having deleted the ligands. Enhanced MD did show some tendency to sample more open-like conformations. To summarize these results, even with enhanced MD, apo HPPK does not sample ternary complex-like conformations, and ternary complex HPPK (with HP and the ATP mimic deleted) does not sample apo-like conformations.

Because apo HPPK does not fluctuate to closed-like conformations, in this work we will consider HPPK−ATP as the basic species of the investigation. Simulations of HPPK−ATP (hereafter, we use this notation as shorthand for the complex of HPPK, ATP, and the two Mg^{2+} ions that are required for the catalytic activity) have been carried out to answer the following two sets of questions: (1) What happens to the ATP along a path that spans the ternary complex to apo forms? Does ATP release from the protein at some stage along a closed (ternary complex-like) to open (apo-like) path, or are there sufficient interactions with the protein that it always remains bound to HPPK? Said otherwise, does HPPK−ATP provide a large conformational ensemble? (2) Once an open conformation of HPPK−ATP is achieved, will ATP still remain bound to HPPK? Can conventional MD address this issue, or are enhanced MD methods required?

If these issues are to be addressed by atomistic-based methods in the complex configuration space of a protein with its ligands, where conventional MD cannot guarantee good sampling in a reasonable computational time, methods that accelerate the exploration of configuration space must be introduced. A number of methods exist that speed up transitions over potential energy barriers. One class of method introduces restraints that operate on the atoms to direct the trajectory between some initial and final state.[39] The restraints can range from being applied to all of the atoms to drive the system between the (known) end points with complete conformity to being applied to just a particular atom−atom distance as would be appropriate for obtaining a one-dimensional potential of mean force. Another approach uses the parallel tempering/replica exchange method (REM)[13−21] and its variants.[20,21] The REM method is global; for example, in the original temperature REM, where replicas of the system are simulated with temperatures larger than the ambient one, all degrees of freedom are "targeted" for enhanced sampling speed through the use of the higher temperatures. Another approach is to use a reweighting method, which modifies the potential surface to generate a trajectory that more readily surmounts barriers.[22−28] The trajectory is then reweighted back at each step to restore Boltzmann sampling. We developed a version of reweighting that we will refer to as targeted reweighting.[28] The term targeted implies that rather than modify the entire potential surface, only very specific terms in the potential are to be modified. Targeting can provide the flexibility to address different impediments to overcoming specific barriers on the potential energy surface. Targeted reweighting can be viewed as the opposite extreme of the global, temperature REM.

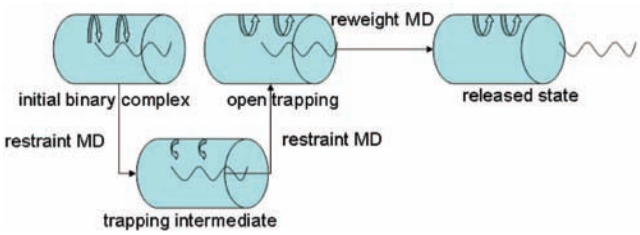

Figure 1. A schematic representation of the MD simulation protocol. The cylinder denotes residues that form a binding region for ATP with key residue side-chain orientations denoted by curved arrows. ATP is represented as a wiggly line. The initial HPPK−$ATPMg_2$ binary complex is constructed from the ternary crystal structure. Ten consecutive restraint simulations direct HPPK−$ATPMg_2$ toward the apo crystal structure. $ATPMg_2$ remains bound throughout the process even though residues initially trapping $ATPMg_2$ gradually move away, through trapping intermediates, until reaching open trapping states. The reweight simulation then shows that $ATPMg_2$ can separate from HPPK through a series of breaking and making hydrogen bonds and salt bridges.

In this study, a combination of a restraint method and a targeted reweight method will be used to address the issues raised above about the mechanism of HPPK−ATP binding. The MD simulation protocol is summarized in Figure 1. The cylinder denotes a set of residues that form a binding pocket for ATP (represented as a wiggly line) with orientations of key residue side-chains that are important for binding ATP denoted by curved arrows. The initial HPPK−ATP binary complex is based on the ternary crystal structure. Restraint simulations are used to direct HPPK−ATP toward the apo crystal structure. The simulations show that ATP remains bound throughout the process even though residues initially trapping ATP gradually move away, through ATP trapping intermediates, until reaching ATP trapping states that have an apo-like HPPK structure. ATP is still held in trap states by a network of hydrogen bonds and salt bridges that operate between ATP−$2Mg^{2+}$ and a number of HPPK core residues. The reweight simulation that starts from this last trap state then shows that ATP can separate from HPPK through a series of breaking and making hydrogen bonds and salt bridges.

The difficulties we found in either opening holo-HPPK or closing apo-HPPK with even enhanced MD methods, in the absence of the restraint/reweight approaches used here, suggest that less atomistic, reduced potential energy methods may be useful. One approach, the elastic network model (ENM),[40−42] uses a harmonically expanded, simplified potential energy function to obtain the normal modes of a protein based on a structural model from, for example, crystallography. Despite the simplicity of the ENM, it has been shown to give reasonable agreement with protein B factors, and to reproduce the low order modes as obtained using atomistic MD force fields by normal-mode analysis. It also can give indications of conformational changes that correspond to directions of closing of an enzyme over its substrates.[41] Thus, we will apply the ENM method to both the apo and the ternary structures of HPPK.

2. Methods

2.1. Molecular Dynamics Simulations. The CUKMODY protein molecular dynamics code, which uses the GROMOS96[43] force field, was used to carry out the simulations. It was modified to incorporate the reweight method as discussed below.

All simulations were run at 303 K under fixed number, volume, and temperature (NVT) conditions.[44] The simulations were carried out in a cubic box with sides of 64.1 Å, having 7671 waters added after waters overlapping the protein were removed. For the evaluation of the electrostatic and the attractive part of the Lennard-Jones energies and forces, the PME method was applied with a direct-space cutoff of 9.0 Å, an Ewald coefficient of 0.32, and a 72 × 72 × 72 reciprocal space grid. Five Na cations were added to neutralize the system. Bonds lengths were constrained with SHAKE,[45] allowing a 2 fs time step, and the temperature was globally controlled with a Berendsen thermostat[46] with a relaxation time of 0.2 ps.

The MD starting structure was obtained from the crystal structure (PDB entry 1q0n) of the ternary complex of *E. coli* HPPK with AMPCPP (an ATP analog that prevents turnover) and two associated magnesium cations, and HP (6-hydroxymethyl-7,8-dihydropterin),[33] by removing the HP and replacing AMPCPP by ATP. The two Mg^{2+} cations were each covalently linked to an oxygen phosphate atom of ATP. One magnesium, designated as Mg1, is linked to an α phosphate oxygen, and the other is linked to a γ phosphate oxygen, designated as Mg2, in accord with their placement in the crystal structure. The ATP phosphates were assumed fully deprotonated (ATP thus has a total charge of −4) in agreement with the ATP protonation state when ligated to Mg^{2+}.[47] The protonation states of the ionizable residues were set to their normal ionization states at pH 7, and 5 sodium cations were added to neutralize the complex. Simulations of the apo HPPK structure were based on the crystal structure[32] (PDB entry 1hka) and were carried out with an analogous protocol.

2.2. Restraint Method. For the restrained MD simulations that were used to transit the protein configuration between two desired conformations, restraints on distances between mass centers of paired atom groups were introduced. Harmonic restraint potentials $V = (k/2)(x - x_0)^2$ with force constant $k = 2$ kcal/mol/Å^2 were used to restrain the current distance x to be around a desired target distance x_0. A small restraint force constant was used to permit the HPPK−ATP complex to fluctuate extensively without being dominated by the effects of the restraints. The restraints were applied in a stepwise manner, by dividing the transition between the initial and final states into 10 sequential windows. Each consisted of 500 ps of MD simulation with restraints set as stated above with $x_0 = n(x_{\text{final}} - x_{\text{initial}})/10 + x_{\text{initial}}$, n the window number running from 1 to 10, and $x_{\text{final}} = x_{\text{apo}}$ and $x_{\text{initial}} = x_{\text{close}}$ denoting a distance in the apo and closed (the ternary complex with HP removed) crystal structures, respectively.

All of the trajectory data analysis was carried out with ANALYZER,[48] a program written for the purpose of analyzing trajectory data by a wide variety of methods. In particular, the RMSD and RMSF measures and all figures requiring superposition of trajectory frames were carried out with ANALYZER. All trajectory snapshots were superposed to the backbone atoms of the core residues of HPPK. In accord with the crystal structure designation,[32] loop 1 is defined as residues 9−13, loop 2 as residues 44−53, and loop 3 as residues 82−93. The core consists of the remaining residues.

2.3. Reweight Method. The reweight method[22,24−28] to accelerate configurational sampling is based on the following identity[28] for a Boltzmann average (with potential V) of any function $A(q^N)$ of the system configuration, q^N:

$$\langle A(q^N)\rangle = \frac{\int \mathrm{d}q^N A(q^N) e^{-\beta V(q^N)}}{\int \mathrm{d}q^N e^{-\beta V(q^N)}} = \frac{\int \mathrm{d}q^N \{A(q^N) e^{+\beta\Delta V(q^N)}\} e^{-\beta V^*(q^N)}}{\int \mathrm{d}q^N \{e^{+\beta\Delta V(q^N)}\} e^{-\beta V^*(q^N)}} = \langle A(q^N) e^{+\beta\Delta V(q^N)}\rangle^* / \langle e^{+\beta\Delta V(q^N)}\rangle^* = \frac{\lim_{T\to\infty} \int_{t_0}^{t_0+T} A(q_*^N(s)) e^{+\beta\Delta V(q_*^N(s))}\,\mathrm{d}s}{\lim_{T\to\infty} \int_{t_0}^{t_0+T} e^{+\beta\Delta V(q_*^N(s))}\,\mathrm{d}s} \quad (1)$$

where $V = (V + \Delta V) - \Delta V \equiv V^* - \Delta V$ defines V^*, a modified potential energy surface upon which the dynamics is carried out, $\langle..\rangle^*$ denotes an average with modified (V^*) weighting, and $q_*^N(s)(t_0 \le s \le t_0 + T)$ denotes the V^*-modified trajectory over the simulation time interval, T. The last identity indicates that, with the assumption of ergodicity, the ensemble averages are to be evaluated as time averages over the trajectories generated from the modified surface. At each step of the dynamics on the modified surface, the data can be "re-weighted" with the factor $\exp(\beta\Delta V)$ to guarantee that the average is Boltzmann weighted. If barriers are reduced by use of the modified potential surface, the modified trajectory will explore the configuration space more rapidly.

If the total potential is modified multiplicatively, then this simply corresponds to changing the temperature of the simulation and corresponds to a global method where all degrees of freedom are treated equally. At the other extreme, only specific terms in the potential energy are targeted, and these terms are chosen on the basis of specific information such as the presence of strong electrostatic interactions corresponding, for example, to salt bridges between residues or what we still will refer to as salt bridges between charged portions of ATP and the magnesium cations and ionized residues.

For specific atoms i and j to be targeted, we use a linear scaling of the potential, $V_{ij}^* = \lambda V_{ij}$. A number of λ values were tried. The actual results are quite sensitive to the λ value chosen with too large a value (closer to 1) leading to no effect and too small leading to a release that is so rapid that the sampling is very poor. The choice of $\lambda = 0.71$ led to escape on the nanosecond time scale. The stages that are found took about 1 ns for this choice, and the simulation was run for a total of 2 ns to make sure that ATP, once unbound, did not rebind.

The Ewald[39] method, used in our MD program, requires the system to be electrically neutral. Thus, in general, a direct inclusion of the scaling factor into the Ewald calculation is hard to implement because it would require finding an overall neutral set of interactions to scale. (The Ewald method calculates energy and forces in reciprocal space that is atom-based versus the real space part that is interaction-based.) Because the modified potential surface does not have to correspond to a real surface, this is not, in principle, a problem; however, as in any modified potential method, if the trajectory becomes too distorted from the true potential trajectory, the reweight method becomes counterproductive. To deal with this issue, because we will only target interactions within the protein and/or ATP, and these interactions are dominant within the same MD image cell, the potential modification will only be applied to the primary cell and the real space energy and forces. For example, to target an electrostatic interaction between atoms labeled 1 and 2, the interaction energy V_{12} and corresponding atom forces F_1 and F_2 are calculated using the Ewald method with $\lambda = 1$, which is just the normal Ewald MD procedure. Next, the differences between using $\lambda = 1$ and using the scale factor λ are calculated directly from Coulomb's law in the primary cell as $V_{12}^{\mathrm{diff}} = (\lambda - 1)(q_1 q_2 / r_{12})$, and the corresponding forces F_1^{diff} and F_2^{diff} are obtained by differentiation. Next, the above differences are added to the Ewald V_{12}, F_1, and F_2 calculated before to obtain the net values $V_{12}^{\mathrm{net}} = V_{12} + V_{12}^{\mathrm{diff}}$, $F_1^{\mathrm{net}} = F_1 + F_1^{\mathrm{diff}}$, and $F_2^{\mathrm{net}} = F_2 + F_2^{\mathrm{diff}}$. These net forces are used to advance the system configuration, and the net energy is used to obtain ΔV. The other (van der Waals and internal) interaction terms can be obtained by a similar scheme.

2.4. Elastic Normal Mode Method. The normal modes are evaluated from a Hooke's law potential function $V = \sum_{r_{ij}<R_c} c(r_{ij} - r_{ij}^0)^2$, where the r_{ij} are pair distances referenced to their "equilibrium" values r_{ij}^0 (from the crystal structure), and the sum is carried out over all pairs within a cutoff radius R_c. The force constant $2c$ is assumed the same for all pairs. This potential function is diagonalized to obtain the modes as implemented in the *elNémo* Web server, the Web interface to *The Elastic Network Model* at http://igs-server.cnrs-mrs.fr/elnemo/. The default settings are used for the analysis. There are six zero frequency modes corresponding to translational and rotation, and the subsequent modes are ordered by their eigenvalue size starting with the smallest.[49]

3. Results

3.1. Restraint MD of the Binary Complex. The molecular dynamics simulations are based on the *E. coli* ternary complex of HPPK, AMPCPP with two magnesium cations and HP, with HP removed and AMPCPP replaced by ATP (see the Methods for preparation and MD simulation details). The fully deprotonated ATP phosphates (total charge −4) with the two ligated Mg^{2+} cations provide a neutral, although highly polar, ligand for HPPK. A previous 7 ns conventional MD simulation of this binary complex led to little change in conformation from the ternary (closed) structure. Furthermore, in other work,[50] we carried out simulations using a Hamiltonian replica exchange method[20,21] to see if HPPK by itself, again started from the ternary crystal structure with both ATP and HP removed, would take on a more apo-like conformation, but these simulations also led to modest rearrangements. For these reasons, we focus on the HPPK−ATP binary complex and use another approach that introduces a particular set of restraints to drive the loops toward a conformation similar to the apo structure. Restraints were picked partly on the basis of the observation that long side-chains of some of the loop 3 residues (principally Arg82, Arg88, and Trp89) are draped over the ATP when HPPK is closed, forming a cylinder whose front face is composed of these residues, as schematized in Figure 1. These side-chains should be pushed out toward the solvent in conformity with the apo crystal structure. Other restraints were chosen to try to make the backbone conformation of loops 2 and 3 similar to that of the apo crystal structure. To achieve this transformation, harmonic restraints (with force constant $k = 2$ kcal/mol/Å^2) on 15 distances, measured between the mass centers of the atom pairs listed in Table 1, were introduced. The restraints were applied in a stepwise manner, by dividing the transition from the HPPK−ATP closed to open form into 10 sequential phases, with each phase consisting of 500 ps of MD, to interpolate between the end points.

Figure 2 displays a superposition of representative structures selected from three of the 10 above 500 ps time intervals corresponding to windows 1, 5, and 10. From the figure, we see that the cores of the three structures are well-aligned, which suggests that even under the forces arising from converting

TABLE 1: Atom(s) Whose Distances Are Used for the Restraint Simulations

atom(s) 1	atom(s) 2
CA[a] Gly46	CA Asp97
CA Pro47	CA Asp97
CA Asp49	CA Asp97
CA Arg82	CA Asp97
CA Arg84	CA Asp97
CA Ala86	CA Asp97
CA Arg88	CA Asp97
CA Trp89	CA Asp97
CA Arg92	CA Asp97
CZ[b] Arg82	CA Asp97
CZ Arg84	CA Asp97
CZ Arg88	CA Asp97
CZ Arg92	CA Asp97
CZ[c] Arg92	CA Leu78
CE2[d] Trp89	CA Asp97

[a] CA denotes a C-α atom. [b] CZ stands for the ε carbon and amino groups of the Arg side-chain. [c] This restraint was not used during the 10-window restraint procedure, but was later realized to be important to ATP separation from HPPK. It was added later, while holding the loops open in the tenth window. [d] CE2 denotes a carbon atom of the 6-member aromatic ring.

Figure 2. Superposition of representative structures from three windows along the restraint pathway from closed to open. The structure for window 1, which is quite similar to the closed form, is colored in yellow; the structure for window 5 is colored in purple; the structure for window 10 is colored using the normal convention. ATP in each window is shown in "ball and stick" mode, and residues Arg82 and Trp89 are shown in "stick" mode. ATP remains bound to HPPK throughout the restraint simulation.

HPPK−ATP from its closed to open forms, there is minimal perturbation of the core, again showing the stability of the protein core. By comparing the loop conformations (including both backbone and important side-chain conformations, such as Arg82, Arg88, and Trp89), it is clear that loops 2 and 3 were pulled gradually from closed-oriented to open-oriented conformations. In particular, the side-chains of Arg82, Arg88, and Trp89 that point inward to seal ATP in the binding pocket of the closed form progressively move to point out to the solvent in the open form. Another key feature to note is that the ATP position is very stable along the trajectory, with all its parts hardly moving. Our initial supposition was that once the side-chains that cover part of ATP in the closed form move away ATP might have separated from HPPK. That this did not happen

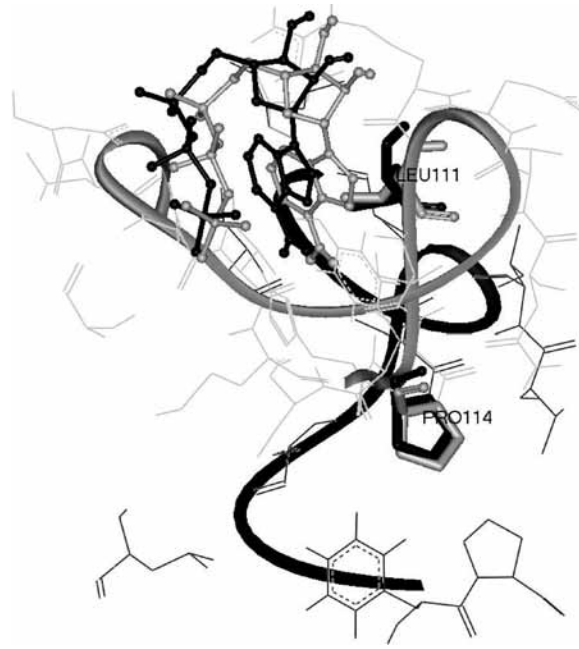

Figure 3. The adenosine recognition site, with residues whose centers are within 10 Å of the adenine CA4 and CA5 atoms (the common atoms of the adenine bicycle). Leu111 and Pro114, the central recognition residues identified from the ternary complex and apo crystal structures,[33] are displayed showing that between window 1 (closed) and 10 (MD-open) their positions are invariant while many other residues have undergone substantial conformational changes. Window 1 is in gray, and window 10 is in black.

suggested that there must be other interactions responsible for maintaining ATP bound to HPPK in the absence of HP.

The binding pocket for ATP is also responsible for the specificity of HPPK to ATP relative to other nucleotides. Residues responsible for adenosine specificity were identified by Yan and co-workers[33] by comparing the apo and ternary crystal structures and looking for residues around the adenosine whose conformations hardly changed between these two structures. In this fashion, Leu111 and Pro114 were identified as key recognition residues, and they each were considered the centers of hydrophobic sets of residues. That this specificity should be maintained for the range of conformations sampled along the restraint pathway should be a good indicator of the ability of these conformations to be robust ATP traps. Figure 3 displays the residues whose centers are within 10 Å of the adenine CA4 and CA5 atoms (the waist of adenine) for restraint windows 1 and 10. The Leu111 and Pro114 positions are extremely stable, although many other residues within the search range have clearly moved a great deal to make the transition from closed to open HPPK.

To further study the interactions responsible for binding ATP to HPPK, a 9 ns MD simulation was carried out starting from the end configuration of the above stepwise restraining procedure. The restraints as listed in Table 1 were still maintained with equilibrium distances set to be equal to the ones measured from the apo HPPK crystal structure. This simulation was carried out to see if ATP would leave the active site automatically when HPPK was restrained to its apo-like state. In Figure 4 (left panel), a CPK view of the HPPK X-ray closed structure is shown for comparison with the CPK view of the protein structure after holding the restraints for 9 ns (right panel). Two points are worth noting. One is that from the viewpoint of the figure, it is clear that there is nothing blocking the pathway of releasing the ATP in the right panel picture, while the path of releasing ATP in

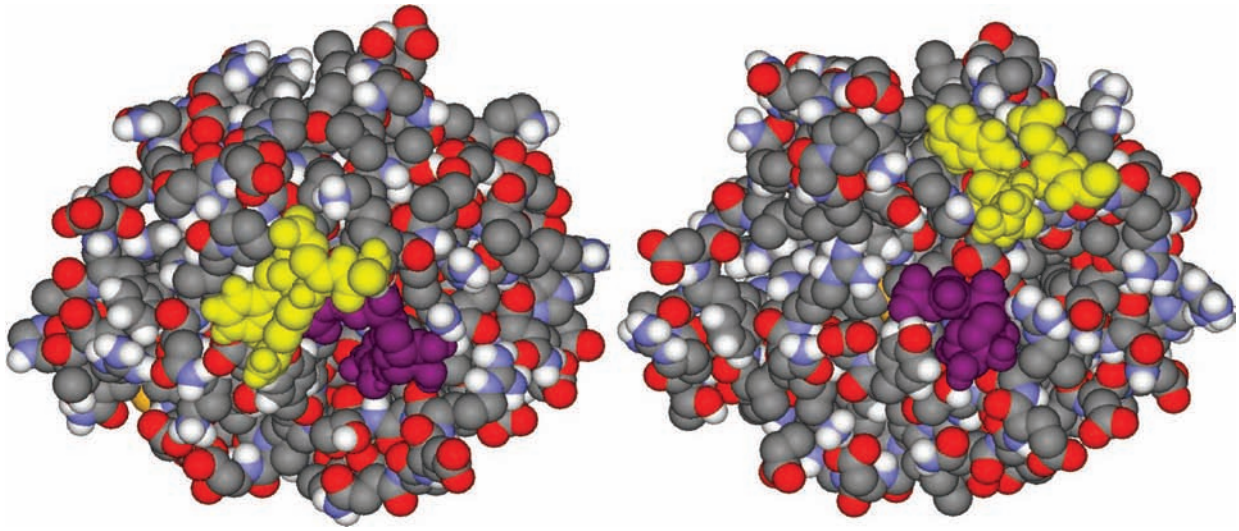

Figure 4. (left panel) CPK view of the starting MD simulation structure derived from the ternary complex. (right panel) CPK view of the MD structure after maintaining the restraints for 9 ns subsequent to the restraint opening protocol. ATP is colored purple. The yellow residues, 86−89, which cover part of ATP in the initial ternary complex, are mainly replaced by solvent interactions in the MD-opened structure.

the left panel picture is blocked by Ala86, Glu87, and the side-chains of Arg88 and Trp89. For clarity, these four residues are colored yellow. The other point is that there is minimal difference between the two pictures with respect to the ATP center of mass position relative to the protein core, although the conformations of ATP in the two figures are a bit different. (The conformation for the MD snapshot shown in the right panel is more compact in comparison with the X-ray structure shown in the left panel.)

3.2. Reweight MD of the Binary Complex. Clearly, the ATP−HPPK interactions are sufficiently strong that on an MD time scale (here 9 ns) ATP remains bound, even though the interactions present in the closed structure that are certainly designed to hold ATP in position are absent in the MD-open form. To attempt to release ATP, one could use a scheme similar to what was just used to open HPPK−ATP. However, to do so either requires initial and final states as given by, for example, crystal structures, or if an obvious path does exist the ligand could be pushed out with restraints in an appropriate direction. We have used the latter scheme successfully in other contexts.[51] However, here, an appropriate path is not clear from, for example, the end of the restrained open simulation. More importantly, picking a particular path will certainly introduce a prejudice into the simulation that may or may not be realistic. Thus, as noted in the Methods, when specific interactions can be identified, targeted reweighting is an appropriate and more objective choice to accelerate the exploration of configuration space that here is characterized by the ATP−HPPK interaction.

In both the closed form crystal structure and the MD opened structure, the two magnesium cations are very close to the carboxylate groups of two HPPK core residues, Asp95 and Asp97. For example, in the MD opened structure, the distances of Mg1 (associated with the α phosphate of ATP) to the closest carboxylate oxygens of Asp95 and Asp97 are 2.5 and 3.0 Å, and the corresponding distances for the Mg2 (associated with the γ phosphate of ATP) are 3.3 and 4.6 Å. Even though the side-chains of Arg82, Arg88, and Trp89 no longer sequester ATP, there still are strong interactions with the protein, notably with the carboxylate groups of core residues Asp95 and Asp97, and these strong "salt bridges" are good candidates for important barriers restraining $ATP^{4-}(Mg^{2+})_2$. Unscreened charge interactions that are on the scale of 100 kcal/mol are essentially as strong as covalent bonds and will clearly prevent the movement of ATP on any normal MD time scale. Therefore, these salt bridges were subjected to the targeted reweighting scheme discussed in the Methods. The targeted atoms are the carbon and two oxygens of the carboxylate groups in these two residues and both magnesium cations; thus, the Mg1 and Mg2 to Asp95 and Asp97 electrostatic interactions are targeted. A uniform scaling value of $\lambda = 0.71$ (see Methods) was used. The modified trajectory was started up from an end point configuration of the tenth restrained simulation.

The targeting leads to ATP separating from HPPK on the nanosecond time scale. Six stable states were found along the path. The stable states are defined by examining the reweight energy, the electrostatic energy between the two magnesium cations and the two residues, along the trajectory. They correspond to plateaus in this energy. The initial modified energy of interaction V^* is ∼300 kcal/mol, while at the final state it is ∼30 kcal/mol. The energy scale is so large that we were not successful in carrying out the reweighting required to obtain the correct Boltzmann populations along the trajectory. That would be necessary if a potential of mean force were the objective, but the modified trajectory still provides states along the path, as is explained in more detail in the Discussion.

Six representative structures from the trajectory were picked for display to show different states as ATP separates, and their superposed pictures are shown in Figure 5. The first structure (ATP in yellow) is the starting structure (end of the tenth restrained simulation), and the sixth one (ATP in red) is where ATP has moved out of the binding pocket. The middle four structures (the ATP is colored green, blue, purple, and orange, respectively) are stable states along the path. The gradual exit of ATP is evident from Figure 5, and it is accomplished through a combination of mass center movement and rotation of the ATP, although it is difficult to see details of the motion from this figure. Therefore, the relevant hydrogen bonds and salt bridges were analyzed for the first five representative structures, and the results for structures 1, 3, and 5 are shown in Figure 6 that displays hydrogen bonds (left panels) and salt bridges (right panels) and are listed in Table 2 (hydrogen bonds) and Table 3 (salt bridges). Between the starting structure (structure 1) and structure 2, the mass center position of ATP does not change much, while its conformation does change significantly so that

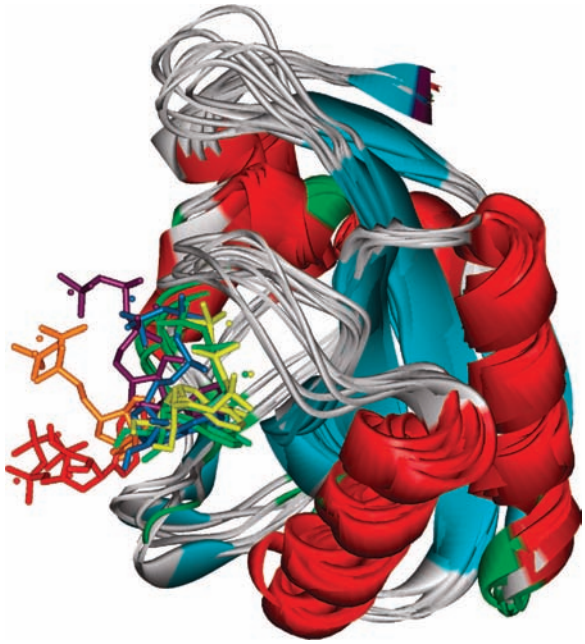

Figure 5. $ATPMg_2$ for six different conformations as it separates from HPPK are shown with yellow, green, blue, purple, orange, and red, indicating stages 1−6. The gradual separation of ATP is evident as a combination of reorientational and translational motion.

three new hydrogen bonds were formed and the two salt bridges involving one of the two Mg ions, Mg2, were broken. Between structure 2 and structure 3, ATP moved along its path away from the binding pocket somewhat; whereby three old hydrogen bonds and one salt bridge were broken, while one new hydrogen bond and one new salt bridge were formed. It is noteworthy that ATP has changed its conformation somewhat so that some old hydrogen bonds and salt bridges can be preserved with the change of its mass center position. This aspect of ATP motion is in evidence during the whole process. Throughout the movement from structure 3 to structure 4, although ATP underwent a large mass center position change, three of the four old hydrogen bonds were preserved, and the one that was broken was replaced by a new one with similar character. For the salt bridges, the one between Mg1 and Asp97 was lost, while the one between ATP and Arg110 changed a little bit. Again, although ATP moved a large step down its path (monitored by the energy of interaction with Asp95 and Asp97) of moving away from the binding pocket, during the transition from structure 4 to structure 5, only one old hydrogen bond was broken, while all three other hydrogen bonds and all the salt bridges were preserved. Finally, the ATP−HPPK energetic interaction decreased to its smallest value and ATP moved to positions (see Figure 5 with ATP in red) where it is essentially out of the HPPK binding pocket.

3.3. Elastic Normal Mode Analyses of HPPK. In view of the problems that even the HREM MD methods have in either opening HPPK based on the ternary complex structure, or closing apo-HPPK toward the ternary complex structure, less computer intensive methods based on simplified potential functions treated harmonically may be of use. The elastic network model (ENM)[40−42] uses a harmonic potential that is based on interactions in a finite sphere around each atom center. There are instances where normal mode-based analyses of an apo protein structure will have modes that point to more closed forms.[41] For example, Temiz et al.[52] studied the open and closed forms of adenylate kinase with a form of ENM. Adenylate kinase has two domains (LID and AMPbd) that are open in the apo form and must close to sequester its substrates. They found that the lowest mode of the apo form describes a closing motion of the LID domain toward the AMPbd domain required for ligand binding. The ligand bound form analysis exhibits a more restricted motion, which may be involved with dissociation of the ligand−protein complex.

We used the *elNémo* Web server (see Methods) to carry out ENM on the apo and the ternary complex forms of HPPK. The ENM on the ternary complex protein atoms was carried out to see if there was evidence for the directions required for loop opening. The ternary-complex-based ENM exhibits high connectivity and, as such, does not make a significant distinction between the core and loop regions of HPPK. The connectivity of an ENM mode is a measure of atom participation in the mode, with a large value indicating that many atoms are involved.[49] These features are consistent with the known[33] rigidity of the protein in the ternary complex. There is no evidence for an opening pathway of HPPK based on this analysis, a feature that has been noted in a normal mode-based study of adenylate kinase.[52]

The ENM based on the apo form has most of the atom motions concentrated in the loop regions, which is consistent with the core stability and loop motion found in all of our MD simulations. Among the first five modes, two (modes 4 and 5) are flagged as low connectivity by *elNémo*, which indicates that they are well concentrated in the loop regions, especially loop 3. The lowest (nonzero) frequency mode, mode 1, corresponds to loop 2 and 3 motions that has loop 2 moving in while loop 3 moves out; thus, this mode is not of interest for a closing type motion. Mode 2 has loops 2 and 3 moving in and out coherently and, potentially, could be applicable to describing a closing motion. In Figure 7, we display the X-ray 1HKA (apo) and 1Q0N (ternary complex) structures along with four of the mode 2 snapshots. It is important to note that in ENM calculations, while the mode directions are known from diagonalizing the potential energy function, the mode amplitude is arbitrary. The corresponding atom displacements of a given mode are only for the purpose of illustration of a possible motion; the actual motion may be much smaller than that illustrated. There is some evidence in Figure 7 for loop closure toward the ternary structure loop positioning. The actual motion of loop 3 that is required to go from open to closed consists of a translation and a twist. Mode 2 does not capture the twist motion. An examination of other modes, in particular the local ones, 4 and 5, does show a twist for loop 3 in mode 5, but it is not in the correct direction.

These visual features can be made more quantitative by examining the cumulative mode overlap between the modes and the difference $\Delta R = R^{holo} - R^{apo}$ between ternary and apo HPPK structures: $\Delta R = R^{holo} - R^{apo} = \sum_{\nu}^{3N} (\Delta R \cdot m_{\nu}^{T}) m_{\nu} \equiv \sum_{\nu}^{3N} a_{\nu} m_{\nu}$. The overlap coefficients[49] $l_{\nu} = a_{\nu}/(|m_{\nu}||\Delta R_{\nu}|)$ are normalized versions of the a_{ν}. Large l_{ν} would indicate motion in the desired direction. The cumulating overlaps for the first five modes are (0.000, 0.061, 0.061, 0.068, 0.068). Thus, mode 2 does indicate some tendency for closing in the correct direction among the first five modes, but it is still rather small.

4. Discussion

The simulations discussed in this work with both normal and various enhanced MD sampling methods were carried out with the goal of investigating the role of protein fluctuations in the trapping and binding of ATP to HPPK. The hypothesis that proteins sample a range of conformational states spanning apo to holo-like conformations, and will trap ligands in a broad range

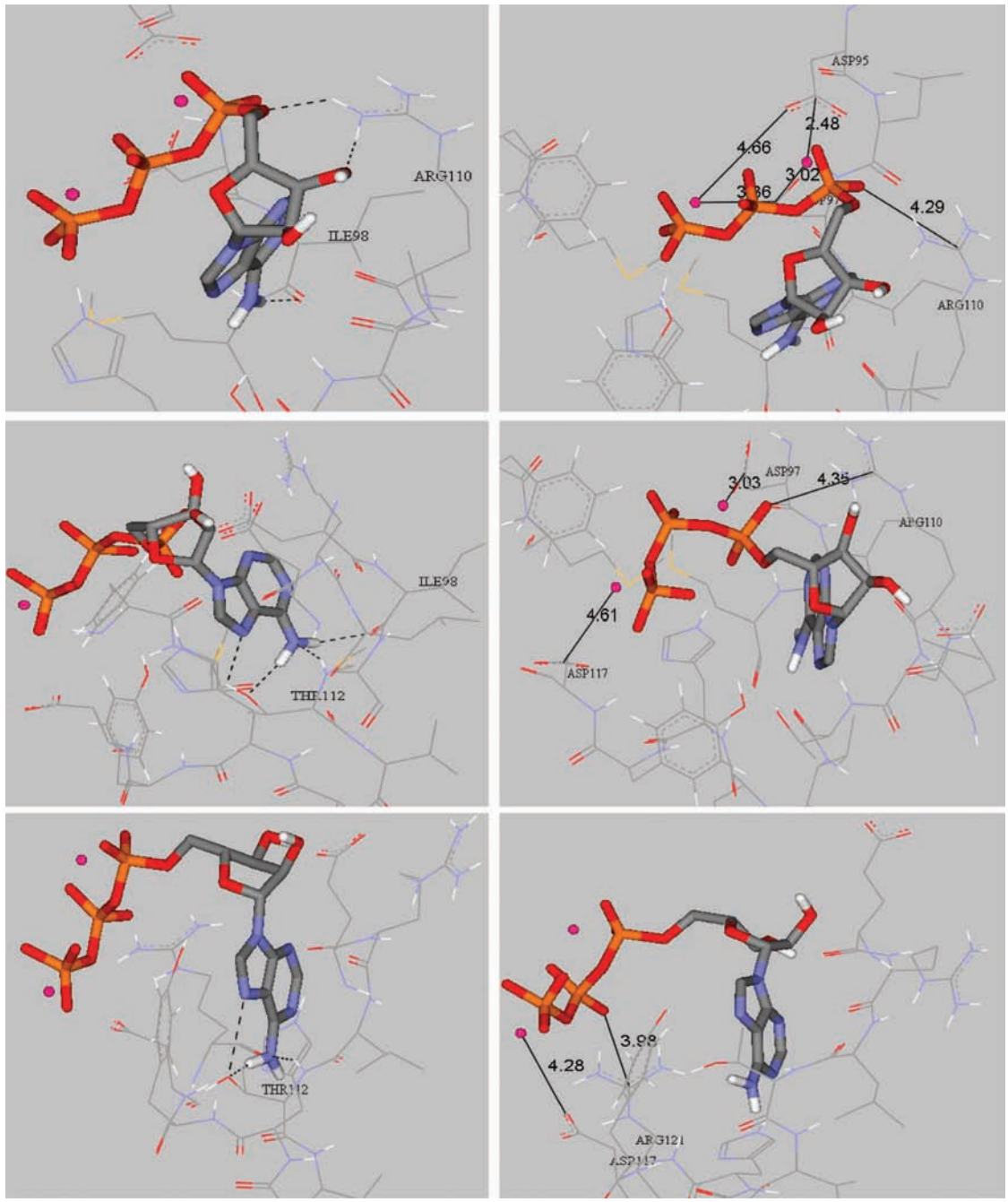

Figure 6. Details of the hydrogen bond and salt bridge interactions as ATP separates from HPPK. Left panels, from top to bottom, are hydrogen bonds (dotted lines) for stages 1, 3, and 5. Right panels are the corresponding salt bridges (solid lines). See Table 2 for hydrogen bond and Table 3 for salt bridge particulars.

of conformations, is attractive from the perspective that this scenario should have a lower energy requirement than other mechanisms of ligand binding.

A minimal set of restraints was found that did lead to HPPK−ATP opening to apo-like conformations. One scenario that could have resulted during the restraint simulation was that at some point along the 10 stages used to span the closed to apo-like conformations ATP would have been separated from HPPK. This was not found. Instead, as shown in Figure 2, the relative center of mass position between HPPK and ATP hardly changed, even though several residues present in the ternary structure that clearly block ATP from solvent exposure have moved away from the ATP to be essentially solvated in the last restraint window, as in the apo crystal structure (see Figure 4). Additionally, the conformations along the opening path maintain the network of residues that permit the adenine recognition machinery of HPPK to operate, as illustrated in Figure 3. These results suggest that many conformations of HPPK spanning from closed to open can trap ATP. The strong salt bridge interactions between $ATPMg_2$ and HPPK over a broad range of HPPK conformations are responsible for the trapping. As noted in the Introduction, this is a form of conformational selection whereby ATP−HPPK is present over a broad conformational space that, when in the more closed forms, is then suited to binding HP.

To investigate the interactions responsible for binding ATP to HPPK in these open conformations, we first carried out a 9 ns conventional MD run (with the restraints maintained at the last window values) starting from the end point of the HPPK−ATP restraint simulations (Figure 2), and we found that

TABLE 2: Hydrogen Bonds That Are Present in the Stages of ATP Separation from HPPK

	hydrogen bond	
structure number	atom of ATP	atom of HPPK
structure 1 (starting structure)	AN6 (nitrogen)	carbonyl oxygen of Ile98
	AO3 (oxygen)	terminal nitrogen on guanidine group of Arg110
	AO5 (oxygen)	terminal nitrogen on guanidine group of Arg110
structure 2	AN6 (nitrogen)	carbonyl oxygen of Ile98
	AN6 (nitrogen)	carbonyl oxygen of Thr112
	AN7 (nitrogen)	backbone nitrogen of Thr112
	AO3 (oxygen)	terminal nitrogen on guanidine group of Arg110
	AO5 (oxygen)	terminal nitrogen on guanidine group of Arg110
	AO2PG (oxygen)	oxygen of the phenol group of Tyr116
structure 3	AN6 (nitrogen)	carbonyl oxygen of Ile98
	AN6 (nitrogen)	oxygen of the hydroxide of Thr112
	AN6 (nitrogen)	backbone nitrogen of Thr112
	AN7 (nitrogen)	oxygen of the hydroxide of Thr112
structure 4	AN6 (nitrogen)	carbonyl oxygen of Met99
	AN6 (nitrogen)	oxygen of the hydroxide of Thr112
	AN6 (nitrogen)	backbone nitrogen of Thr112
	AN7 (nitrogen)	oxygen of the hydroxide of Thr112
structure 5	AN6 (nitrogen)	oxygen of the hydroxide of Thr112
	AN6 (nitrogen)	backbone nitrogen of Thr112
	AN7 (nitrogen)	oxygen of the hydroxide of Thr112

TABLE 3: Salt Bridges That Are Present in the Stages of ATP Separation from HPPK

	salt bridge[a]	
structure number	group 1 (positively charged)	group 2 (negatively charged)
structure 1 (starting structure)	Mg1	carboxylate group of Asp95
	Mg1	carboxylate group of Asp97
	Mg2	carboxylate group of Asp95
	Mg2	carboxylate group of Asp97
	guanidine group of Arg110	α-phosphate group of ATP
structure 2	Mg1	carboxylate group of Asp95
	Mg1	carboxylate group of Asp97
	guanidine group of Arg110	α-phosphate group of ATP
structure 3	Mg1	carboxylate group of Asp97
	Mg2	carboxylate group of Asp117
	guanidine group of Arg110	α-phosphate group of ATP
structure 4	Mg2	carboxylate group of Asp117
	guanidine group of Arg121	β-phosphate group of ATP
structure 5	Mg2	carboxylate group of Asp117
	guanidine group of Arg110	β-phosphate group of ATP

[a] Mg1 (Mg2) refers to the one associated with the β (γ) phosphate of ATP.

ATP still remains bound to HPPK. Examination of the simulation data, illustrated by Figure 4, shows that there are several residues (Asp95 and Asp97) that still interact strongly with $ATP^{4-}(Mg^{2+})_2$. These core residues are clearly part of the binding pocket for ATP and provide a large, mainly electrostatic, interaction with $ATP^{4-}(Mg^{2+})_2$. In view of the specific salt-bridge-like interactions between these charged residues and the magnesium cations that in turn have a strong electrostatic interaction with ATP^{4-}, some of these interactions were the natural candidates to use in a targeted reweight scheme. The targeted reweighting does lead to the separation of ATP from HPPK as shown in Figures 5 and 6 and detailed in Tables 2 and 3. The successive and staged breaking of the original hydrogen bonds and salt bridges and formation of new ones

Figure 7. The apo crystal structure (1HKA) in green, the ternary complex crystal structure (1Q0N) in yellow, and 4 snapshots from mode 2 of the ENM (in normal colors). Loop 3 is indicated by ALA86 and loop 2 by PRO47. The ENM predicts that both loops have a closing motion, but, as evident from the figure, especially for loop 3, the twisting motion to close over the active site is not described.

dominate the interactions for ATP binding. In terms of energetics, there are six stages of energetic interaction that can be identified over about 1 ns of simulation time, and then, over the remaining 1 ns of the simulation, the ATP remains separated from HPPK. Thus, these salt bridges play a key role in the binding mechanism.

The simulations can rationalize the equilibrium and kinetic data on ATP (AMPPCP) binding to HPPK. First, the equilibrium data showed that HPPK binds AMPPCP with high affinity. Second, without the presence of ATP, HPPK does not bind HP in measurable quantities. Both of these facts are consistent with a large conformational ensemble of HPPK−ATP. Third, the kinetics indicates that ATP binds first, and slowly, followed by very rapid HP binding.[38] The kinetic data are consistent with a scheme where formation of a binary complex of HPPK−ATP occurs first and suggests that a "proto-pocket" for HP binding is formed by this event for conformations that are in the vicinity of the ternary complex. That ATP binding is slow may be a consequence of ATP selecting from a conformational ensemble, although, of course, it could also be a consequence of a large barrier to complex formation. Once ATP is bound, the HPPK−ATP complex may stabilize to a set of conformations appropriate for the rapid uptake of HP. Consistent with this scenario is that in the product complex, where the pyrophosphate group has been transferred to form HPPP, the product release is slow and rate limiting.[35] The charged pyrophosphate group may act in a fashion similar to that of ATP and lead to the slow product release.

The refractory nature of HPPK on MD accessible time scales suggests that faster, more qualitative methods of exploring

conformational changes would be profitable. To that end, the ENM calculations were pursued. Not surprisingly, in view of the rigid ternary structure, the ENM analysis provided modes that are distributed among most of the protein atoms and are not well suited to predicting an opening pathway. The apo ENM analysis did provide modes with atom participation concentrated in the loops, especially loops 2 and 3. There is a mode whose direction of motion somewhat describes a closing pathway, but examination of the direction that it predicts for loop 3, as well as the overlap with the ternary structure, shows that it is only qualitatively correct. Examination of the loop motions in HPPK required for closing shows that the loop backbone movement is not very large. Rather, it involves large-scale reorientation of residues with long side-chains, principally Arg82 and Arg88, and of Trp89. Thus, in contrast with, for example, adenylate kinase where closing requires large domain movements, HPPK closing is a more local event and, furthermore, may be strongly influenced by its ligands.

The introduction of restraints introduces the danger that, if too many are used, the system cannot adequately sample a realistic configuration space that is dictated by the potential energy function, while if too few are used the desired motion will not be obtained. Thus, some minimal set of restraints should be chosen that are physically motivated. That was accomplished here with the use of restraints that were picked on the basis of an examination of the ternary and apo crystal structures.

A reweight scheme does not directly provide dynamical information relevant to the original potential surface. So, one should not get the impression from the reweight simulation that ATP can be released from HPPK on the nanosecond time scale. There are methods available[53−55] that can take the dynamics on the modified surface V^* and reconstruct rates for the original potential surface based on, for example,[54] obtaining a potential of mean force for the relevant reaction coordinate. We were not successful in reweighting back the trajectory to obtain the correct Boltzmann equilibrium sampling. Said otherwise, a potential of mean force was not obtained because the large range in energies of the modified potential surface V^* along the trajectory did not permit the collection of sufficient data for the required accurate. This problem stems from the exponential dependence on the reweight potential ΔV evident in eq 1. The only way to address the problem would be to scale many more degrees of freedom and possibly obtain a smaller range of energy values. However, those more implicit degrees of freedom (in contrast with the explicit salt-bridge interactions that we identified) would be very hard to identify. Ultimately, the difficulty is the very high-dimensional surface that is being explored. Furthermore, particular to any binding problem, there is an entropic component to the solvation process, sometimes referred to as a "cratic" entropy effect, requiring separation to infinity of ligand and protein.[56] That is hard to account for in a potential-based MD simulation that only can locally separate ATP from HPPK due to the finite size simulation cell. The targeted reweight method, despite these difficulties, is still a very effective method when explicit degrees of freedom can be identified as key impediments to the slow sampling property of MD.

In conclusion, by use of a combination of restraint and reweight extensions of molecular dynamics, a picture of how ATP interacts with HPPK emerges that rationalizes some of the experimental observations and suggests that the conformational plasticity of enzymes does play a role in ligand binding.

Acknowledgment. A generous grant of computer time from the Michigan State University High Performance Computing Center is gratefully acknowledged.

References and Notes

(1) Kumar, S.; Ma, B. Y.; Tsai, C. J.; Sinha, N.; Nussinov, R. *Protein Sci.* **2000**, *9*, 10.
(2) James, L. C.; Tawfik, D. S. *Trends Biochem. Sci.* **2003**, *28*, 361.
(3) Goh, C. S.; Milburn, D.; Gerstein, M. *Curr. Opin. Struct. Biol.* **2004**, *14*, 104.
(4) Bahar, I.; Chennubhotla, C.; Tobi, D. *Curr. Opin. Struct. Biol.* **2007**, *17*, 633.
(5) Ma, B. Y.; Kumar, S.; Tsai, C. J.; Nussinov, R. *Protein Eng.* **1999**, *12*, 713.
(6) Bryngelson, J. D.; Onuchic, J. N.; Socci, N. D.; Wolynes, P. G. *Proteins: Struct., Funct., Genet.* **1995**, *21*, 167.
(7) Dill, K. A.; Chan, H. S. *Nat. Struct. Biol.* **1997**, *4*, 10.
(8) Changeux, J. P.; Edelstein, S. J. *Science* **2005**, *308*, 1424.
(9) Berg, B. A.; Neuhaus, T. *Phys. Lett. B* **1991**, *267*, 249.
(10) Hansmann, U. H. E.; Okamoto, Y.; Eisenmenger, F. *Chem. Phys. Lett.* **1996**, *259*, 321.
(11) Lyubartsev, A. P.; Martsinovski, A. A.; Shevkunov, S. V.; Vorontsov-Velyaminov, P. N. *J. Chem. Phys.* **1992**, *96*, 1776.
(12) Lyubartsev, A.; Laaksonen, A. *Appl. Paralled Comput.* **1998**, *1541*, 296.
(13) Swendsen, R. H.; Wang, J. S. *Phys. Rev. Lett.* **1986**, *57*, 2607.
(14) Geyer, C. J. Markov Chain Monte Carlo Maximum Likelihood. In *Computing Science and Statistics: Proceedings of the 23rd Symposium on the Interface*; Keramidas, E. M., Ed.; Interface Foundation: Fairfax Station, 1991.
(15) Sugita, Y.; Okamoto, Y. *Chem. Phys. Lett.* **1999**, *314*, 141.
(16) Hansmann, U. H. E.; Okamoto, Y. *J. Comput. Chem.* **1997**, *18*, 920.
(17) Wang, J. S.; Swendsen, R. H. *Prog. Theor. Phys. Suppl.* **2005**, 317.
(18) Hukushima, K.; Nemoto, K. *J. Phys. Soc. Jpn.* **1996**, *65*, 1604.
(19) Lei, H.; Duan, Y. *Curr. Opin. Struct. Biol.* **2007**, *17*, 187–191.
(20) Fukunishi, H.; Watanabe, O.; Takada, S. *J. Chem. Phys.* **2002**, *116*, 9058.
(21) Su, L.; Cukier, R. I. *J. Phys. Chem. B* **2007**, *111*, 12310.
(22) Liu, Z.; Berne, B. J. *J. Chem. Phys.* **1993**, *99*, 6071.
(23) Berne, B. J.; Straub, J. E. *Curr. Opin. Struct. Biol.* **1997**, *7*, 181.
(24) Wenzel, W.; Hamacher, K. *Phys. Rev. Lett.* **1999**, *82*, 3003.
(25) Hornak, V.; Simmerling, C. *Proteins: Struct., Funct., Genet.* **2003**, *51*, 577.
(26) Hamelberg, D.; Mongan, J.; McCammon, J. A. *J. Chem. Phys.* **2004**, *120*, 11919.
(27) Hamelberg, D.; McCammon, J. A. *J. Am. Chem. Soc.* **2005**, *127*, 13778.
(28) Cukier, R. I.; Morillo, M. *J. Chem. Phys.* **2005**, *123*, 234908.
(29) *Chemistry and Biochemistry of Folates*; Blakley, R. L., Benkovic, S. J., Eds.; John Wiley & Sons, Inc.: New York, 1984; Vol. 1.
(30) Walsh, C. *Antibiotics, Actions, Origins, Resistance*; ASM Press: Washington, DC, 2003.
(31) Walsh, C. *Nat. Rev. Microbiol.* **2003**, *1*, 65.
(32) Xiao, B.; Shi, G. B.; Chen, X.; Yan, H. G.; Ji, X. H. *Structure* **1999**, *7*, 489.
(33) Blaszczyk, J.; Shi, G.; Yan, H.; Ji, X. *Structure* **2000**, *8*, 1049.
(34) Xiao, B.; Shi, G.; Gao, J.; Blaszczyk, J.; Liu, Q.; Ji, X.; Yan, H. *J. Biol. Chem.* **2001**, *276*, 40274.
(35) Li, G. Y.; Felczak, K.; Shi, G. B.; Yan, H. G. *Biochemistry* **2006**, *45*, 12573.
(36) Yang, R.; Lee, M. C.; Yan, H. G.; Duan, Y. *Biophys. J.* **2005**, *89*, 95.
(37) Elber, R.; Karplus, M. *J. Am. Chem. Soc.* **1990**, *112*, 9161.
(38) Bermingham, A.; Bottomley, J. R.; Primrose, W. U.; Derrick, J. P. *J. Biol. Chem.* **2000**, *275*, 17962.
(39) Frenkel, D.; Smit, B. *Understanding Molecular Simulation: From Algorithms to Applications*; Academic: San Diego, 1996.
(40) Tama, F.; Sanejouand, Y. H. *Protein Eng.* **2001**, *14*, 1.
(41) Tama, F. *Protein Pept. Lett.* **2003**, *10*, 119.
(42) Tozzini, V. *Curr. Opin. Struct. Biol.* **2005**, *15*, 144.
(43) van Gunsteren, W. F.; Billeter, S. R.; Eising, A. A.; Hünenberger, P. H.; Krüger, P.; Mark, A. E.; Scott, W. R. P. *Biomolecular Simulation: the GROMOS96 manual and user guide*; Vdf hochschulverlag AG an der ETH: Zürich, 1996.
(44) Essmann, U.; Perera, L.; Berkowitz, M. L.; Darden, T.; Lee, H.; Pedersen, L. G. *J. Chem. Phys.* **1995**, *103*, 8577.
(45) Ryckaert, J. P.; Ciccotti, G.; Berendsen, H. J. C. *J. Comput. Phys.* **1977**, *23*, 327.
(46) Berendsen, H. H. C.; Postma, J. P. M.; Gunsteren, W. F.; DiNola, A.; Haak, J. R. *J. Chem. Phys.* **1984**, *81*, 3684.

(47) Wang, P. M.; Izatt, R. M.; Oscarson, J. L.; Gillespie, S. E. *J. Phys. Chem.* **1996**, *100*, 9556.
(48) Lou, H. *Analyzer*, 1.0 ed.; East Lansing, 2005.
(49) Suhre, K.; Sanejouand, Y. H. *Nucleic Acids Res.* **2004**, *32*, W610.
(50) Su, L.; Cukier, R. I. in preparation.
(51) Yao, L. S.; Yan, H. G.; Cukier, R. I. *Biophys. J.* **2007**, *92*, 2301.
(52) Temiz, N. A.; Meirovitch, E.; Bahar, I. *Proteins: Struct., Funct., Bioinf.* **2004**, *57*, 468.
(53) Chen, L. Y.; Horing, N. J. M. *J. Chem. Phys.* **2007**, 126.
(54) Hamelberg, D.; Shen, T.; McCammon, J. A. *J. Chem. Phys.* **2005**, 122.
(55) Voter, A. F. *Phys. Rev. Lett.* **1997**, *78*, 3908.
(56) Gilson, M. K.; Given, J. A.; Bush, B. L.; McCammon, J. A. *Biophys. J.* **1997**, *72*, 1047.

JP808664K